The Astronomical Journal, 128:674–686, 2004 August

A *HUBBLE SPACE TELESCOPE* WFPC2 INVESTIGATION OF THE DISK-HALO INTERFACE IN NGC 891[1]

Jörn Rossa[2] and Ralf-Jürgen Dettmar
Astronomisches Institut, Ruhr-Universität Bochum, Universitätsstrasse 150/NA7, D-44780 Bochum, Germany; jrossa@stsci.edu, dettmar@astro.rub.de

René A. M. Walterbos
Department of Astronomy, New Mexico State University, MSC 4500, Box 30001, Las Cruces, NM 88003; rwalterb@nmsu.edu

and

Colin A. Norman[2]
Department of Physics and Astronomy, Johns Hopkins University, 3400 North Charles Street, Baltimore, MD 21218; norman@stsci.edu
Received 2004 February 10; accepted 2004 May 12

ABSTRACT

We present deep narrowband observations with high spatial resolution of extraplanar diffuse ionized gas in the halo of NGC 891, obtained with the WFPC2 on board the *HST*. Our Hα observations, centered on the northern part of NGC 891, reveal an extended gaseous halo, which fills almost the entire field of view of our WFPC2 observation. Whereas NGC 891 has been studied extensively with ground-based telescopes, here the small-scale structure of the extended emission-line gas is presented at a high spatial resolution of 0.″1, corresponding to 4.6 pc at the distance to NGC 891. The majority of the Hα emission is diffuse. Several discrete features (e.g., filaments) are visible as well. Some of the filaments reach distances of up to 2.2 kpc above the galactic plane and are extremely collimated, even at high galactic latitudes. We compare the morphology of these filaments with theoretical models, which describe possible transport mechanisms in a general way. Despite the prominent dust lane, many bubbles, shells, and supershells can be discerned in the midplane. We also investigate extraplanar dust features, which are best visible in unsharp-masked images of our broadband F675W image, and we compare them with the spatial distribution of DIG filaments. The high-$|z|$ dust is detected out to distances of 2.2 kpc above/below the galactic midplane. Individual dust features, however, are not spatially correlated with diffuse ionized gas counterparts, such as individual filaments. Quite interestingly, the orientation of the dust features changes from being mostly aligned perpendicular to the disk at low galactic latitudes to a parallel alignment at high $|z|$. We compare the diffuse ionized gas distribution to the hot ionized medium, traced by X-ray observations performed by *Chandra*. There exists a good correlation of the presence of the warm and hot ionized gas: in particular, an X-ray bright region at $|z| \sim 1$–1.5 kpc fills the entire northern halo region, whereas the intensity in the midplane is considerably depressed. We also compare the sizes of individual Hα emission line features in the midplane of NGC 891 with similar structures that are known in our Milky Way and in the LMC.

Key words: galaxies: halos — galaxies: individual (NGC 891) — galaxies: ISM — galaxies: spiral — galaxies: structure

1. INTRODUCTION

The detection of extended diffuse ionized gas (DIG), or frequently also called warm ionized medium (WIM), in halos of late-type spiral galaxies is generally believed to be correlated with the star formation (SF) activity in the galaxy disk. This H^+ layer in external galaxies is equivalent to the *Reynolds layer*, which is observed in our Milky Way (Reynolds 1984). More recent galactic studies showed that the diffuse Hα emission is ubiquitous and detected in almost every direction on the sky (Haffner et al. 2003). DIG has a typical electron density of $n_e \approx 0.1$ cm^{-3} in the disk (decreasing exponentially toward higher galactic latitudes) and has a typical scale height of 1–2 kpc.

In the theoretical picture the gas, most likely driven by collective supernovae (SNe), is expelled into the halos of these galaxies. Norman & Ikeuchi (1989) developed the theory in which the gas is being transported through tunnel-like features into the halo, called *chimneys*, provided the superbubbles created from SNe fulfill the breakout criterion. Depending on the strength of the gravitational potential, the gas may be able to fall back onto the galactic disk, which is described as the *galactic fountain* scenario (Shapiro & Field 1976; de Avillez 2000). A few other investigations of the multiphase interstellar medium involving SNe have been conducted (e.g., Korpi et al. 1999; Wada & Norman 1999, 2001; Wada 2001).

The fractional contribution of DIG to the total Hα emission in galaxies typically reaches values of ≈25%–50% (e.g., Walterbos & Braun 1994; Ferguson et al. 1996b; Lehnert & Heckman 1995; Thilker et al. 2002), and DIG is thus an important constituent of the ISM. The emission is most likely due to photoionization by hot OB stars (Miller & Cox 1993; Dove & Shull 1994). The temperatures, determined from upper limits of diagnostic line ratios (e.g., [N II] lines) in our Galaxy and in a few external galaxies, are in the range of 8000–13,000 K. (Rand 1997; Reynolds et al. 2001; Tüllmann et al. 2000). However, other ionizing and heating mechanisms, such as shock ionization (Chevalier & Clegg 1985), magnetic reconnection (Birk et al. 1998), and turbulent mixing layers (Slavin et al. 1993) have been invoked to account for the observed emission-line ratios, which are not consistent with current pure photoionization models (Mathis 1986;

[1] Based on observations with the NASA/ESA *Hubble Space Telescope*, obtained at the Space Telescope Science Institute, which is operated by the Association of Universities for Research in Astronomy, Inc., under NASA contract NAS5-26555. These observations are associated with proposal 6588.
[2] Space Telescope Science Institute, 3700 San Martin Drive, Baltimore, MD 21218.

Domgörgen & Mathis 1994). The line ratios in the disk are more or less consistent with the models. However, recently determined line ratios in external galaxies, such as those of [O III]/Hα, increase with increasing galactic distance, which is not compatible with these models, as observations have shown (Rand 1998, 2000; Tüllmann et al. 2000).

Furthermore, it is presently not clear how the ionizing photons can travel such vast distances from the disk into the halo, if OB stars are regarded as the primary source. Gaseous halos seem to be a common feature among starburst galaxies (Lehnert & Heckman 1995), where the gas is most likely expelled into the halos by starburst- or SNe-driven superwinds. However, in normal or *quiescent* galaxies the presence of extended gaseous halos does not seem to be the general case but is mostly encountered in late-type spirals with high SF activity on both local and global scales (Rossa & Dettmar 2003a, 2003b).

A few investigations have been undertaken to study the gaseous halos in *quiescent* galaxies (Pildis et al. 1994; Rand 1996; Hoopes et al. 1999; Collins et al. 2000; Rossa & Dettmar 2000; Miller & Veilleux 2003), but not all of these galaxies revealed extraplanar DIG (eDIG). The first larger survey to study eDIG in the disk-halo interaction (DHI) context has been carried out recently, which covered 74 edge-on galaxies (Rossa & Dettmar 2003a, 2003b). It was shown in this investigation that nearly 41% of the survey galaxies have eDIG detections, and a minimal threshold of SF rate per unit area was derived (Rossa & Dettmar 2003a).

A variety of morphological features are generally observed (e.g., filaments, plumes, bubbles, shells), and sometimes in the case of actively star-forming galaxies (e.g., NGC 4700), even a pervasive DIG layer at typical distances of 1–2 kpc above/below the galactic plane was detected. Individual filaments, occasionally reaching distances of up to 6 kpc, are superposed in a few cases as well (Rossa & Dettmar 2003b). Whereas the above-mentioned survey and the smaller samples studied by individual researchers have aimed at the detection and overall morphology of gaseous halos in edge-on galaxies, little is actually known about the small-scale structure of the eDIG. This small-scale structure can only be studied in the nearest galaxies with the highest spatial resolution available. Therefore, high-resolution observations with the *HST* in nearby edge-on spirals, yielding spatial resolutions of the order of a few parsecs, such as in the case of NGC 891, seem promising to study the disk-halo connection in detail.

2. NGC 891 AND THE DISK-HALO CONNECTION

The famous nearby edge-on spiral NGC 891 is considered to be a twin to our own Milky Way in many respects. It is one of the best-studied edge-on galaxies, which has been investigated in almost all wavelength regimes from the radio (e.g., Dahlem et al. 1994) to the X-ray (Bregman & Pildis 1994) regime in the DHI context. About a decade ago an eDIG layer was discovered in this galaxy (similar to the Reynolds layer in our Milky Way) by Dettmar (1990) and Rand et al. (1990) using Hα narrowband imaging. Further spectroscopic investigations confirmed and revealed diffuse emission up to 5 kpc above the galactic plane (Keppel et al. 1991; Dettmar & Schulz 1992; Rand 1997, 1998). From the imaging observations it was shown that the SF activity in NGC 891 is not equally distributed along the disk, since an asymmetrical distribution of the DIG layer is observed. The dominant SF activity is located in the northern part of NGC 891, whereas in the southern part there is much less activity. This is consistent with radio continuum observations (Dahlem et al. 1994), which are not affected by dust. Therefore, extinction can be excluded as a cause of the depression of the eDIG layer in the southern part. Instead, it is a real consequence of the decreasing strength of SF activity within the disk of NGC 891. Those inhomogeneities are not unusual among actively star-forming galaxies.

In addition to bearing a prominent eDIG layer, NGC 891 also shows spectacular extraplanar dust features, which reach up to $z \approx 2$ kpc into the halo as well (Howk & Savage 1997). So far, correlation studies of the DIG distribution traced by the Hα emission exist for the radio continuum (Dahlem et al. 1994), H I (Swaters et al. 1997), and for the hot ionized medium (HIM) as observed in the X-rays (Bregman & Pildis 1994). A previous study by Howk & Savage (1999) showed that there is generally no direct correlation between the DIG filaments and extraplanar dust features on a small scale. This behavior was confirmed by Rossa & Dettmar (2003b) using a much larger sample. A reinvestigation of the extraplanar dust in NGC 891 using deeper broadband images also validates this trend (Howk & Savage 2000). Submillimeter observations performed with SCUBA have detected cold dust within two-thirds of the optical disk of NGC 891 (Alton [1998]), while FIR observations performed with the *ISO* satellite have detected extended cold dust within the whole extent of the optical emitting disk of NGC 891 (Popescu et al. [2004]). In addition, an extended halo has been reported from CO observations obtained with the IRAM 30 m telescope (García-Burillo et al. 1992). All these observations strongly imply a large-scale circulation of matter from the disk into the halo. This is directly linked to galaxy evolution, as the IGM is enriched with metals by those outflows.

The distance to NGC 891, as a member of the NGC 1023 group, has been derived to be 9.5 Mpc (van den Bergh 1992), which is consistent with other distance determinations, such as the planetary nebula luminosity function (PNLF), which yielded 9.9 Mpc (Ciardullo et al. 1991). We will adopt a distance of 9.5 Mpc throughout this paper. With this distance NGC 891 is a prime candidate for high-resolution studies of the small-scale structure of the DIG. Furthermore, this galaxy has an inclination that is very close to be perfectly edge-on ($i \gtrsim 88.^{\circ}6$), where the disk separates from the halo in projection very well. We therefore have carried out Hα observations with the *HST*, making use of the WFPC2, which yielded a spatial resolution of 4.6 pc at the distance of NGC 891. This allowed us to study the distribution of DIG in external galaxies in unprecedented detail. Similar studies have been carried out recently for the starburst galaxy NGC 3079 (Cecil et al. 2001, 2002), where the nucleated gaseous outflowing cone was imaged and compared with the X-ray morphology, studied with *Chandra*. Furthermore, one additional *HST*/*Chandra* comparison study in the case of the interacting actively star-forming Virgo spiral galaxy NGC 4631 was performed (Wang et al. 2001).

3. OBSERVATIONS AND OBSERVING STRATEGY

The *HST* observations of NGC 891 were carried out with the WFPC2 camera. For the narrowband (Hα) observations, the F656N filter was used, and the broadband images (to be used for continuum subtraction) were obtained with the F675W filter. The data sets have the following abbreviations: U54Y0202B (narrowband) and U54Y0101B (broadband). In total, eight *HST* orbits were performed to obtain a deep Hα image of NGC 891, resulting in an on-source integration time of 25.1 ks. The observational parameters are listed in Table 1.

The individual exposures were taken between 1999 February 17–19 in dither mode, to approach more closely the diffraction

TABLE 1
JOURNAL OF OBSERVATIONS

Object	R. A. (J2000.0)	Decl. (J2000.0)	t_{exp} (s)	Filter	λ_m (Å)	FWHM (Å)	P.A. (deg)
NGC 891.....	02 22 39	+42 22 11	4 × 400	F675W	6734.5	889.4	22
NGC 891.....	02 22 39	+42 22 11	8 × 2800	F656N	6561.5	22.0	22
NGC 891.....	02 22 39	+42 22 11	1 × 2700	F656N	6561.5	22.0	22

NOTE.—Units of right ascension are hours, minutes, and seconds, and units of declination are degrees, arcminutes, and arcseconds.

limit of the telescope (since the WFPC2 CCD pixels are undersampled) and to allow good cosmic-ray removal. The WFPC2 field was centered on R.A. $02^h22^m39^s$, and decl. $+42°22'11''$, both J2000.0, at *HST* orientation angle $\phi = 67°$, centered on the PC frame. This resulted in a P.A. $= 22°$ on the sky, thus aligned along the major axis of NGC 891. The field covers the northern part of NGC 891, slightly north off the central region, including parts of the prominent bulge (see Fig. 1). The field position and P.A. were chosen for a variety of scientific reasons, which are briefly elucidated below.

From the detections of the extraplanar gas layer in NGC 891 in the early 1990s, it was known that there is an asymmetrical eDIG distribution, with the prominent gaseous halo in the northern part of NGC 891 (see Dettmar 1990; Rand et al. 1990). Because of the velocity field of NGC 891, which was studied in H I (Rupen 1991), the northern part was also the most suitable choice for our investigation, as it covered the Hα emission in the available F656N filter passband. The southern part of NGC 891 would not be covered by the FWHM of the F656N filter. Furthermore, interesting features (filaments, H II regions) are visible in ground-based images in this specific northern part, which can be studied now with higher angular resolution.

A few orientations of the WFPC2 aperture onto NGC 891 were possible in principle. However, because of the time-critical nature of observations (NGC 891 could only be observed in small periods of time twice a year) and a possible further delay of the WFPC2 observations during 1998 (due to problems associated with the coolant of the NICMOS camera), we were prompted to change our original proposed orientation. After analyzing possible solutions, taking into account the above-mentioned constraints, three viable orientations, which would cover most of the desired areas in NGC 891, remained. We finally decided to choose the $\phi = 67°$ (P.A. $= 22°$) orientation, since the other two orientations suffered from relatively bright stars near the edges of the WFPC2 aperture, which would lead to reflections and ghost images in the WFPC2 field. To avoid contamination of bright stars on the border of these regions (known as the dragon's breath), which would ultimately lead to difficulties in removing artifacts that might be caused by these, we neglected the other two orientations.

4. DATA REDUCTION

The data were pipeline-processed in the usual manner, including bias-level correction and flat fielding. The further reduction was performed using the DRIZZLE package within IRAF, which was developed for dithered images (Fruchter & Hook 2002). First, we applied coarse cosmic-ray removal to the images using the PRECOR task. Then the dithered images were cross-correlated, with one image acting as the reference image, both in the on-band and off-band exposures. Subsequently, we determined the shifts using SHIFTFIND and AVSHIFT , choosing the WF2 field as a weight parameter. The average shifts determined in each of the four WFPC2 CCD chips for each individual exposure had values ranging from -5 to 16 pixels. To check that the count rates in the subfields did not significantly deviate from one image to another, we compared the values, obtained from two selected fields, as determined through the image statistics. The images did not show any significant deviation. Now each of the four PC/WF subimages were processed separately. We then generated cosmic-ray masks. The shifted subimages were drizzled with a scale factor of 0.5 to an embedded output image having the dimension of 2048×2048 pixels. After DRIZZLING the images were median-combined. Then we BLOTTED (the

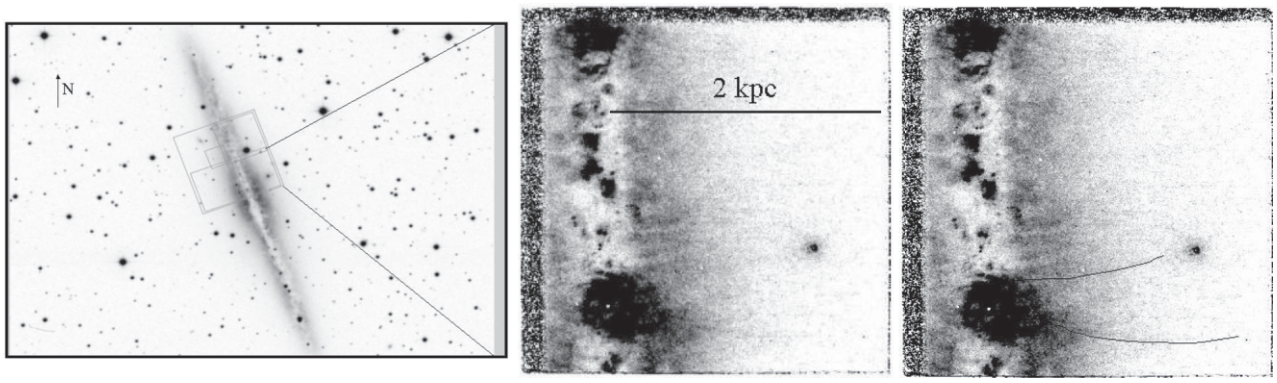

FIG. 1.—NGC 891. The left panel shows a DSS image with the WFPC2 field of view overlaid. The middle panel shows the drizzled continuum-subtracted Hα image of the disk-halo region just north of the bulge (WF3). There are individual long and thin filaments that emanate from a supergiant shell region in the galactic midplane. These filaments reach extraplanar distances of $\sim$2 kpc. The filaments are clearly visible when viewed at different contrast on a computer screen but might be difficult to view in the paper version. For clarity, the right panel therefore shows the same image as the middle panel, but with the filaments overdrawn in black for easy visibility. The most prominent filaments are very narrow, with sizes of $\approx$15 pc. Such morphological structures are not predicted by current theoretical models. Note that the images in the middle and right panels are rotated by 22°, so north is to the northwest quadrant.

process of reverse DRIZZLING) the median image to have images that match the positions and the size of the input images. These blotted images can be used to identify and mask cosmic rays in the original images. Finally, the blotted images were drizzled onto a finer grid. To recover some resolution from the undersampled images, we thus shrank the drop size. For more details on the DRIZZLING method, we refer to Gonzaga et al. (1998).

Since from the DRIZZLED 2048×2048 images no mosaics could be generated within IRAF, we have used the smaller 800×800 images to create a 1600×1600 mosaic, which was used for the flux-calibration comparison and for identifying the bright filaments, whereas the higher resolved DRIZZLED images have been used to analyze the small-scale morphology of the DIG.

5. ANALYSIS

5.1. *Narrowband Imaging*

Because of the given FWHM of 22.0 Å of the F656N filter, the filter passband also contains some amount of continuum. To obtain pure Hα emission, the F656N images had to be continuum-subtracted by the scaled broadband filter (F675W) exposure. This was done by measuring the count rates of several individual stars, which were visible in all of the four WFPC2 fields in both the on-band and off-band exposures. The individual measurements were then averaged to obtain a final scaling factor. The off-band exposure, multiplied by the scaling factor, was subtracted from the on-band exposure to obtain a continuum-free Hα image. Because of the relatively small FWHM of the F656N filter there is no contamination of emission from the adjacent [N II] doublet. Finally, a flux calibration has been performed. The net Hα image's calibration was derived following O'Dell & Doi (1999). We did not include the correction they derive for contamination of [N II] emission, since the velocity shift of NGC 891 places little [N II] emission in the filter passband. The calibration was consistent within the uncertainties with ground-based calibration (Rand et al. 1990). The determined sensitivity of is of the order of emission measure (EM) $= 20$ cm^{-6} pc (rms per pixel).

Generally speaking, using a broadband filter for the continuum subtraction is done to save exposure time in the off-band filter. While the line emission is included in the broad filter passband, the contribution of line emission with respect to the continuum is very small. The equivalent widths of both filter passbands are quite different. Hence, when the continuum image is scaled to the narrowband image to bring the continuum levels together, the line emission in the broadband filter passband is scaled down quite substantially compared with the line emission in the narrowband filter, and very little (a few percent at most) of the line emission may be removed from the narrowband filter passband. Since this data set is primarily geared to the morphology of the emission and not to the diffuse or absolute levels, we opted to use the broadband method to cut back on required exposure time and to maximize the signal-to-noise ratio (S/N).

Galactic contamination of the observed Hα emission in extragalactic sources is feasible in principle, specifically for targets in areas of the sky close to the Galactic plane. For details on the Galactic Hα emission we refer to the emission-line surveys such as WHAM (Haffner et al. 2003), the Virginia Tech Spectral-Line Survey,[3] and the Southern H-Alpha Sky Survey Atlas (Gaustad et al. 2001). Galactic emission could occur, in that [N II] emission from the Milky Way falls in the *HST* filter passband. However, this is unlikely to be a problem. We are discussing a very small region of the sky, and the Galactic emission could only make NGC 891 appear diffuse if it were structured exactly such that it appeared concentrated toward NGC 891's disk, which is what we see in the *HST* and ground-based data. That would seem to be a rather unlikely situation. However, we would like to mention that there is at least one reported case (ESO 209-9), where this can be an issue (Rossa & Dettmar 2003b). We note that ESO 209-9 is closer to the Milky Way Galactic plane in projection and also that the passband of the narrow filter used in that study was much larger than the one in our WFPC2 study.

It should be noted that we cannot make a determination of the total extent of the NGC 891 emission because of the relatively small field of view covered by the WFPC2 observation. For the same reason, we cannot determine the zero level background from our data. This issue can be better addressed by ground-based imaging and long-slit investigations (e.g., Dettmar 1990; Rand et al. 1990; Rand 1997; Hoopes et al. 1999).

5.2. *Broadband Imaging*

The broadband (F675W) images of NGC 891 were obtained for two purposes. The primary aim was to subtract the continuum emission from the on-band images. These images also allow a comparison of extraplanar dust features with eDIG filaments. These two physically distinct phases (see Howk & Savage 2000) of the ISM can be studied in detail to search for possible correlations between the two extraplanar ISM constituents. To better enhance the contrast between the dust structures and the background light from the galaxy, we have constructed unsharp-masked versions of our broadband images. These were obtained by dividing the broadband images by a smoothed version of the broadband images. The latter were created using a Gaussian filtering technique.

6. RESULTS

6.1. *Extraplanar Diffuse Ionized Gas (eDIG)*

The overall distribution of eDIG in the northern part of NGC 891, as derived from our WFPC2 observations, shows a very smooth pattern (see Fig. 2). These narrowband *HST* observations offer the highest spatial resolution of eDIG studied in external *nonstarburst* galaxies to date, with a spatial resolution of 4.6 pc at the distance to NGC 891. Whereas the majority of the high-$|z|$ Hα emission is clearly diffuse, several filaments can be discerned as well. A description of the various eDIG/DIG features (e.g., filaments, plumes/bubbles, H II regions, supershells) including the sizes and distances from the galactic midplane, are summarized in Tables 2 and 3. The nomenclature of our identified eDIG filaments is in the following format: Fil-WF field+number and selected fields. The brightest filaments are marked in Figure 3. The positional offsets Δx and Δy (in arcseconds) relative to the center of the PC field are listed as well. The coordinates for the filaments refer to the observed position from which they seem to originate. For the two arcs, the positional offsets refer to the outermost extension of each arc. As the arcs are irregular in shape, we list the distance to the outermost detected emission, rather than defining a radius, which would be difficult to assess because of their observed morphology. In Figure 4 we show the calibrated image in a logarithmic stretch and with a coordinate grid.

[3] See http://www.phys.vt.edu/~halpha.

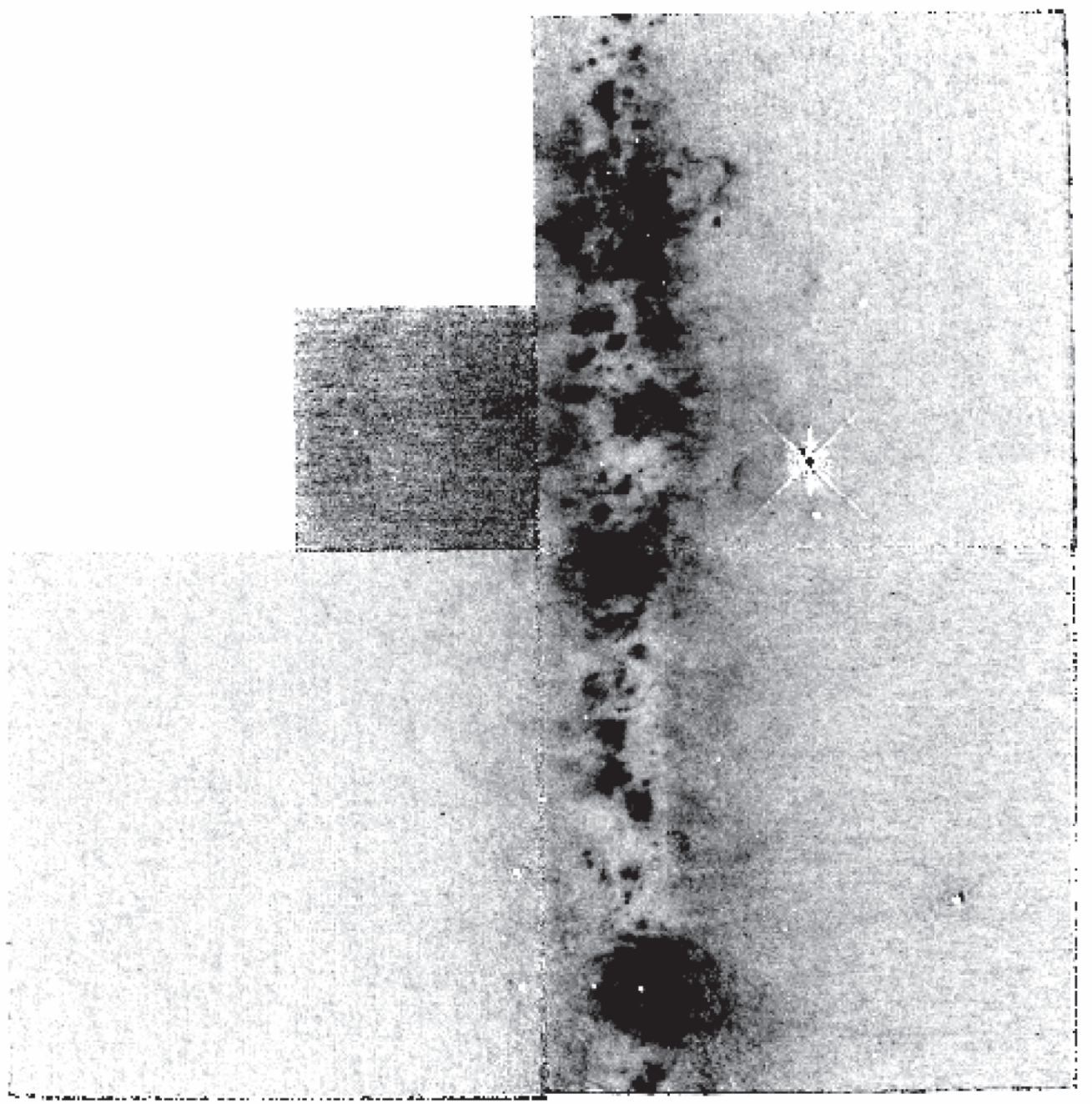

FIG. 2.—Continuum-subtracted F656N (Hα) image of NGC 891, obtained after creating a mosaic from the four individual WF/PC fields. A very prominent DIG layer ($z \sim 1.8$ kpc) can be discerned, with individual superposed filaments protruding from the disk region into the halo. The image size of this L-shaped aperture measures $150'' \times 150''$, representing an area of 6.9 kpc $\times$ 6.9 kpc at the distance of NGC 891. The small PC-field measures $34'' \times 34''$. The spatial resolution is $0''.1$ pixel^{-1}.

6.2. *Morphology of eDIG*

On the larger scale the Hα emission is observed mostly in diffuse emission. The eDIG can be detected out to $|z| \sim 1.8$ kpc above the galactic midplane. We are actually limited by the field size of the WFPC2 and sensitivity. Given the position of NGC 891 on the WFPC2 chip, the field size is about 2.5–4.5 kpc from the midplane to the border of the chip on the western/eastern side. The intensity of the DIG is brightest above the most active disk star-forming regions (e.g., supergiant shells). A few bright filaments and arcs are seen protruding from the regions, where supershells are located in the halo. The two giant arcs that emanate from the bright emission complex in the WF4 field (containing the supershell WF-4-SS1) out to $|z| \sim 1.3$ kpc connect on either side with bright emission regions in the disk region. In several cases we detected smaller filaments that appear to be originating from regions deep within the disk, where no bright emission regions are detected. However, this may be an effect of local extinction, as we cannot determine at which depth the filaments are actually connected to the disk. There could be bright supershells embedded in regions of higher extinction, or these regions could be located in deeper layers within NGC 891's disk. Because of the extinction effects we cannot judge which of the two scenarios is true. However, the presence of filaments appearing at $|z| \geq 500$ pc clearly shows the decreasing influence

TABLE 2
PROPERTIES OF INDIVIDUAL eDIG FEATURES IDENTIFIED IN THE CONTINUUM-FREE Hα IMAGES

Identifier Fil-WFi-j	Δx (arcsec)	Δy (arcsec)	$\lvert z\rvert$ (pc)	Dimensions (pc × pc)	Classification
Fil-WF3-1.....	−42.1	−84.3	2197 ± 5	1561 ± 5 × 15 ± 5	Filament
Fil-WF3-2.....	−44.4	−75.7	1967 ± 5	1552 ± 5 × 46 ± 5	Filament
Fil-WF3-3.....	−39.1	−68.5	921 ± 5	410 ± 5 × 46 ± 5	Filament
Fil-WF3-4.....	−38.2	−68.7	930 ± 5	502 ± 5 × 78 ± 5	Filament
Fil-WF3-5.....	−36.2	−34.3	760 ± 5	451 ± 5 × 46 ± 5	Filament
WF4-EH2.....	−42.4	+29.1	617 ± 5	64 ± 5 × 55 ± 5	Extraplanar H II region
Arc-WF4-1	−45.2	+35.9	760 ± 5	460 ± 5 × 98 ± 5	Arc
Arc-WF4-2	−56.5	+20.4	1271 ± 5	815 ± 5 × 55 ± 5	Arc
Fil-WF3-6.....	−20.2	−63.7	755 ± 5	373 ± 5 × 92 ± 5	Filament
Fil-WF3-7.....	−18.8	−54.0	1368 ± 5	921 ± 5 × 60 ± 5	Filament
Fil-WF3-8.....	−15.8	−18.7	1257 ± 5	713 ± 5 × 50 ± 5	Filament

of extinction at higher galactic latitudes. Scattered light from H II regions contributes only a minor part of the observed DIG emission, as it has been shown from modeling that the contribution at $|z| = 600$ pc falls to about 10% (Ferrara et al. 1996). A profile of the Hα emission in the central emission region perpendicular to the disk of NGC 891 is shown in Figure 5, where the intensity in EM (cm^{-6} pc) is plotted as a function of the spatial distance from the midplane.

Two bright arcs are visible in the WF4 field of the WFPC2, whereby the larger one reaches a distance of $|z| \sim 1.2$ kpc. In the WF3 field two superthin filaments protrude from the disk, and north of them three prominent and thicker filaments are clearly recognizable. On the other side of the disk several fainter filaments emanate from the disk, which are not as straight as the brightest filaments already mentioned.

In a general sense, there is a good correlation of filaments with SF regions in the disk observed. Not only the very thin and long filaments appearing to protrude from the supershells have connections with SF regions in the disk. For instance, there are two bright arcs in the WF4 field (see Fig. 2) that are connected to and actually trace back to the disk, indicative of a galactic fountain scenario. Many of the smaller filaments also seem to originate from bright SF regions within the disk. However, it should be noted that extinction precludes us in several cases from drawing firm conclusions regarding a clear connection.

6.3. *Small-Scale Structure of eDIG*

Although the eDIG distribution in NGC 891 is mostly truly diffuse, numerous filaments and arcs are superposed onto the extended DIG layer. The small-scale structure of these filaments can be investigated down to sizes of about 5 pc. There is no intricate filamentary network observed on the very smallest scales. From the sensitivities obtained we can conclude that a breakup of the diffuse emission can only occur below EM = 20 cm^{-6} pc (rms per pixel) into individual filaments. On the other hand, there are some surprisingly long and superthin (collimated) filaments visible in the WF3 field (see Figs. 1 and 2), which are slightly bent and very collimated even out to very high galactic latitudes. These filaments are barely resolved in ground-based images and have widths of 15 to 50 pc. The one filament (Fil-WF3-2) is coincident with the one previously identified by Howk & Savage (2000) in ground-based WIYN images, which they have dubbed +026+035. From our *HST* observations we have estimated sizes a factor of 2 larger in length and a factor of 3 smaller in width. However, we note that our measurement refers to a mean width, as this filament does not have a constant width as a function of $|z|$. The curved feature marked in Figure 3 as "Artif-1" on the WF4 chip is an artifact caused by the nearby star. In Figure 6 we show an enlargement of the WF4 field, where the two arcs can be seen in more detail. An extraplanar H II region in the disk-halo interface (thick disk) at $|z| \sim 620$ pc is detected, which is indicated by an arrow in Figure 7 (see § 6.6).

6.4. *Structure of DIG Features in the Galactic Midplane*

Although NGC 891 bears a rather prominent and extended dust lane that runs across the galactic midplane (see Fig. 8), several emission regions located in areas not severely influenced by extinction (e.g., individual shells, supergiant shells, H II regions, and SNRs) are visible in our continuum-subtracted Hα images (Figs. 6 and 7). The most spectacular feature in the galactic midplane is the supergiant shell WF3-1-SS1, which measures 677 pc × 824 pc (see Fig. 6). It is similar in size and shape to the supergiant shells found in the LMC (e.g., Meaburn 1980). A superthin ($\Delta x \sim 15$ pc) filament is

TABLE 3
PROPERTIES OF EMISSION FEATURES IN THE GALACTIC MIDPLANE OF NGC 891

Identifier WF-*i*+ID	Δx (arcsec)	Δy (arcsec)	$\lvert z\rvert$ (pc)	Dimensions (pc × pc)	Classification
WF3-1-SS1.....	−31.9	−79.1	134 ± 5	677 ± 5 × 824 ± 5	Supergiant shell
WF3-3-SS2.....	−27.8	−19.8	55 ± 5	700 ± 5 × 511 ± 5	Supergiant shell
WF3-SB-1	−34.1	−31.8	110 ± 5	138 ± 5 × 124 ± 5	Superbubble
WF3-H2-1	−28.2	−43.0	37 ± 5	152 ± 5 × 203 ± 5	H II region
WF3-H2-2	−28.1	−48.7	41 ± 5	226 ± 5 × 230 ± 5	H II region
WF3-H2-3	−31.9	−53.3	134 ± 5	166 ± 5 × 184 ± 5	H II region
WF4-SS-1.....	−32.7	+30.8	170 ± 5	345 ± 5 × 244 ± 5	Supershell

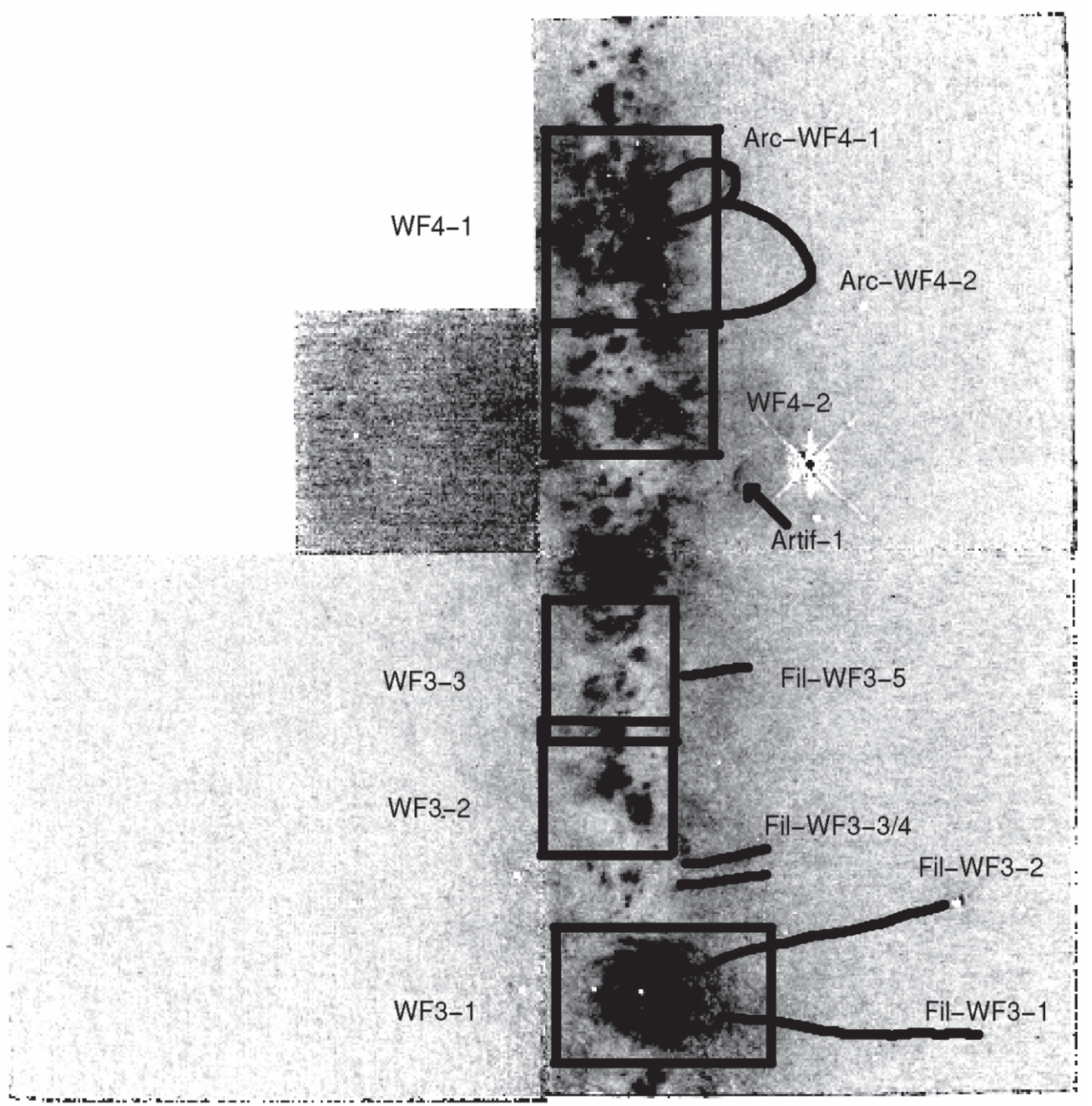

FIG. 3.—Continuum-subtracted F656N (Hα) image of NGC 891, same as Fig. 1. Here several fields are marked, which are shown in the following figures in more detail. Furthermore, the most prominent filaments and arcs are indicated as well. The nomenclature is described in the text.

protruding from this supergiant shell into the halo and reaches a distance of $|z| \sim 1.8$ kpc. A listing of the most prominent emission features in the midplane is given in Table 3, where information on the position within NGC 891 and the physical sizes is given. Individual H II regions are discerned (e.g., Fig. 1), and a superbubble (see Fig. 6) can be identified. In Figures 6 and 7 we have used different gray-scale cuts to accentuate the inner structure more clearly.

In the continuum-subtracted WFPC2 image (Fig. 2) there are local regions (i.e., between the two supershells) that show less pronounced SF activity compared with most other regions. However, this could be attributed either to less SF or to the emission regions being embedded in deeper layers, and hence more affected by extinction. Several filaments emerge from the disk at intermediate distances of about 400 pc above the disk, and this might suggest that there are strong local inhomogeneities in the dust absorption.

6.5. *Extraplanar Dust*

The extraplanar dust in NGC 891 reveals an intricate network of dusty filaments, which reach extraplanar distances of $|z| \sim 2$ kpc. These dusty filaments and features are most visible in our unsharp-masked broadband image (Fig. 8). In Figure 9 we show a more detailed view of the individual dust patches in the two WFPC2 fields (WF3+WF4), as the dust lane is covered in these two fields. As already studied with ground-based telescopes under exceptionally good seeing conditions of 0.″6, Howk & Savage have previously mapped the extraplanar dust in NGC 891 in the *B* band and *V* band (Howk & Savage 1997, 2000) using the WIYN 3.5 m telescope. We can confirm their

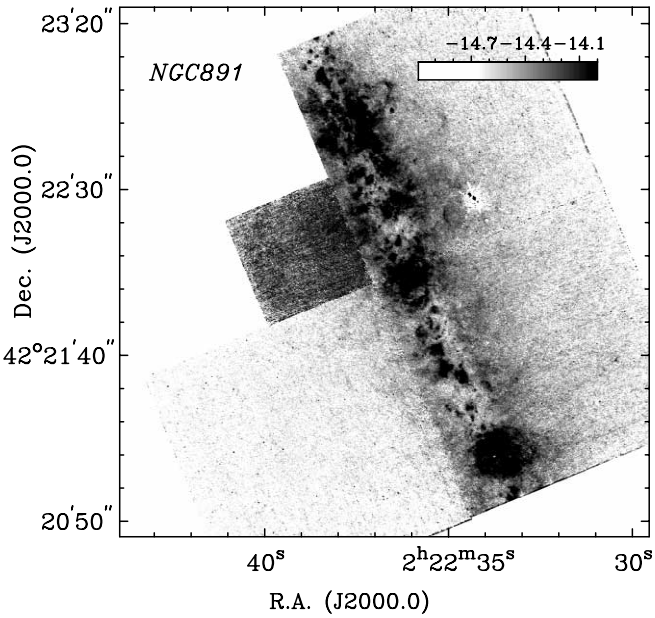

FIG. 4.—Continuum-subtracted F656N (Hα) image of NGC 891. The calibrated image is shown with a coordinate grid and is plotted in a logarithmic stretch in units of ergs s^{-1} cm^{-2} $pixel^{-1}$.

results, and we detect basically the same structure for the extraplanar dust, although our observations were made in the *R* band (F675W), which is somewhat more transparent to dust than their *B* and *V* band. However, the resolution of the WFPC2 is better by a factor of 6, and therefore our dust filaments are better resolved. The structure of the smallest visible dust features on a scale of less than 5 pc can be resolved. The dust filaments show a pronounced substructure that is not well resolved in the WIYN images by Howk & Savage (2000). Interestingly, the high-$|z|$ dust shows basically two different alignments at various scale heights. The very extended high-$|z|$ dust at $|z| \sim 2$ kpc is aligned parallel to the galactic plane, while the dust features at intermediate distances $|z| \sim 0.7$–1.5 kpc are preferentially aligned perpendicular to the disk, although generally a superposition of various directions is observed. As Howk & Savage (1997, 2000) have already given

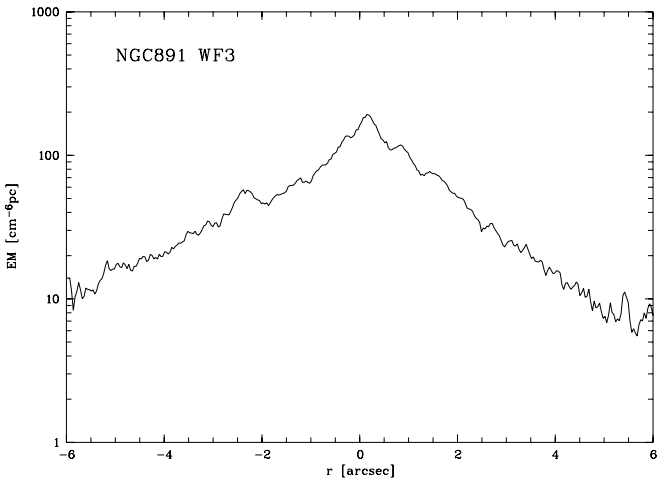

FIG. 5.—Vertical profile of the Hα emission in NGC 891 (plotted logarithmically in units of EM [cm^{-6} pc]) perpendicular to the disk. The cut shows an averaged region (150 pc wide), centered at the bright emission complex at the center of the WFPC2 image (slightly north of the WF3-3 box in Fig. 3).

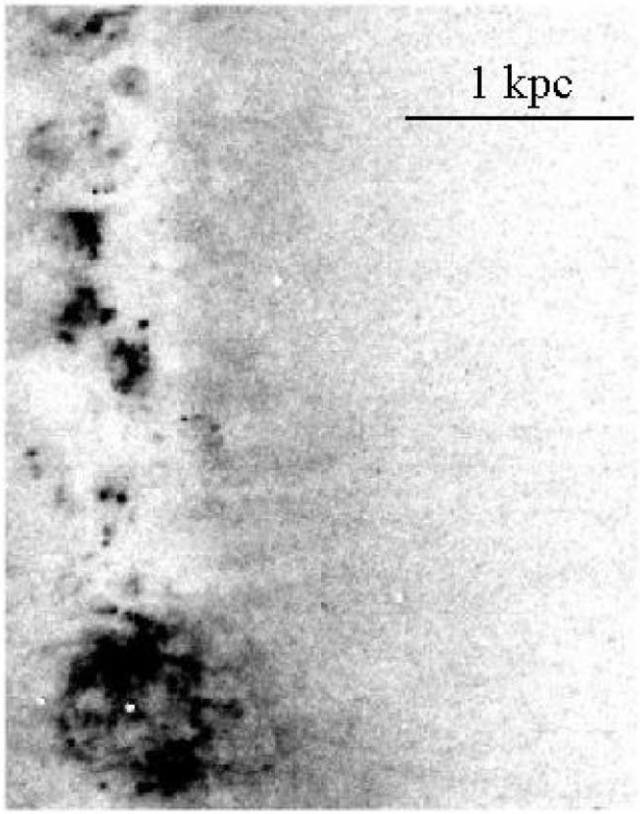

FIG. 6.—Detailed view of the continuum subtracted Hα DIG emission in the WF3 field. On the bottom the supergiant shell WF3-1-SS1 is seen along with other discrete features in the midplane.

an extensive analysis of the individual extraplanar dust features in NGC 891 and our main focus is on the DIG, we refrain here from discussing all further details again.

6.6. *Extraplanar* H II *Regions and Halo PNs*

An interesting side aspect of the detection of Hα emission in the disk-halo interface of spiral galaxies is the search for

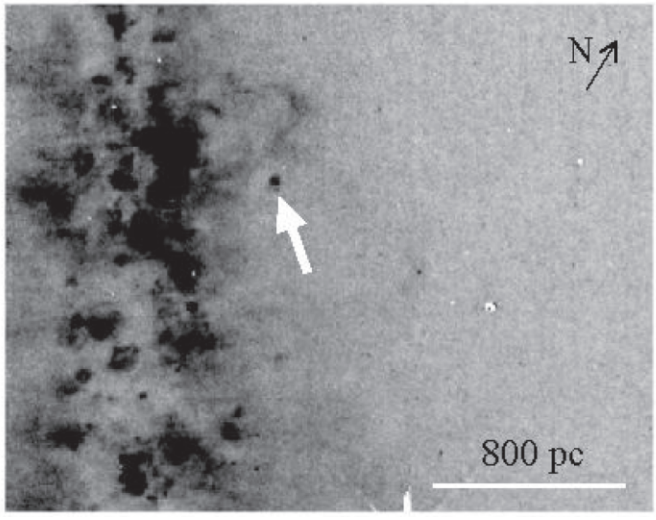

FIG. 7.—Detailed view of the continuum subtracted Hα DIG emission in the WF4 field. Several filaments (some connecting back to the disk) can be discerned. The extraplanar H II region (WF4-EH2) is marked by the white arrow.

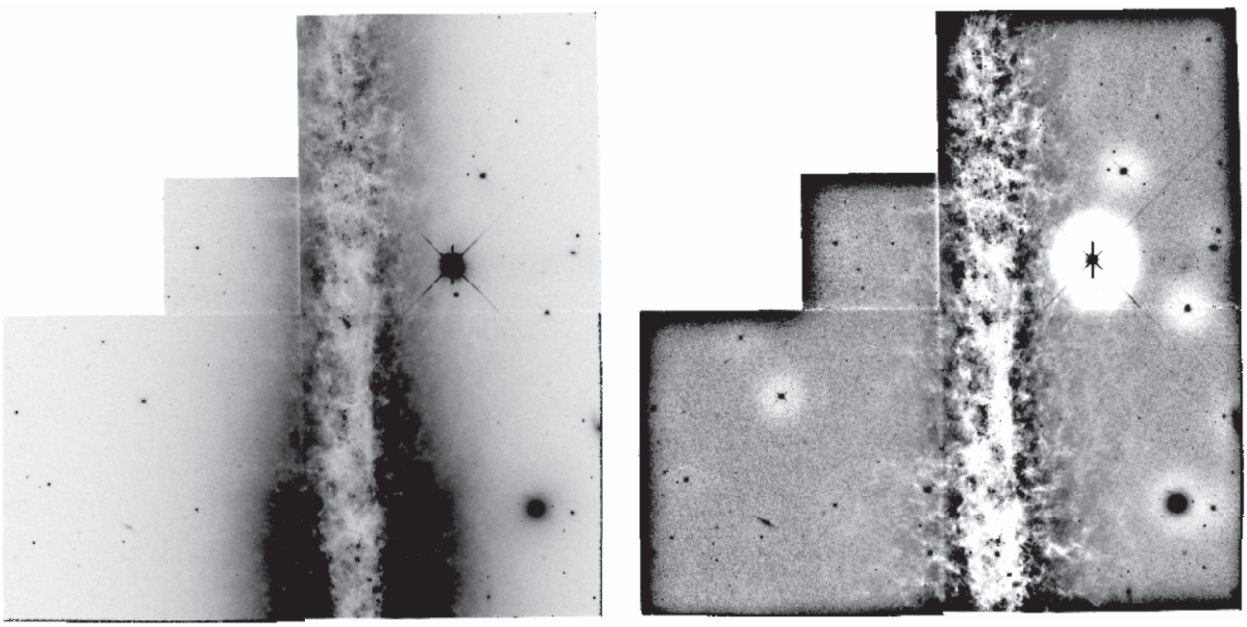

FIG. 8.—*Left*: F675W image. The unsharp-masked broadband image of NGC 891 is shown in the right panel, obtained after dividing the F675W image by a Gaussian-filtered F675W image. High-$|z|$ structures can be identified up to $\sim$2 kpc. While the highest-dust filaments seem to be aligned mostly parallel to the galactic disk, numerous dusty filaments in the region $|z| \sim 1$–1.5 kpc are aligned perpendicular to the galactic disk.

possible extraplanar H II regions giving rise to star formation far above the galactic disk. Over the last couple of years a few detections of extraplanar and intracluster H II regions in and surrounding spiral galaxies have been reported (e.g., Ferguson et al. 1996a; Gerhard et al. 2002; Tüllmann et al. 2003; Ryan-Weber et al. 2004). Specifically, for NGC 891, Howk & Savage (1997) reported a detection of a H II region in the disk-halo interface, dubbed WF4-EH2, which we also identify in our WFPC2 data. It is located at about $|z| \sim 620$ pc above the galactic plane (see Fig. 7). We identify a double morphology, with one knot being much brighter. The size we measured is approximately 45 pc. We note that the knot is much smaller, with some extended diffuse emission around it. We derive a luminosity of $L = 8 \times 10^{36}$ ergs s^{-1}, which is slightly less than the luminosity of the Orion nebula (e.g., Kennicutt 1988). There is a somewhat fainter blotch at a similar distance from the galactic midplane visible in that same figure just south of WF4-EH2, which is probably another H II region. All these observations of extraplanar H II regions establish a low level of star formation at high galactic latitudes. This should be considered when discussing the existence of early-type stars in the Milky Way halo (e.g., Kilkenny et al. 1995; Hambly et al. 1996). However, it should be mentioned that the occurrence of these H II regions is a relatively rare phenomenon; hence, they are unlikely to contribute much, if any, to the ionization of DIG above the disk. Bearing this consideration in mind, it is very unlikely that some or all of the H II regions are due to runaway O stars; for in that case a runaway O star would no longer have an associated H II region.

Another source of Hα emission in the halo is planetary nebulae (PNs). Ciardullo et al. (1991), in their ground-based study of NGC 891, detected a total of 33 PNs in the halo. Of these, 10 PNs are located in our WFPC2 field of view. We show our individual WFPC2 image sections, with the candidate PNs marked by circles, in Figure 10.

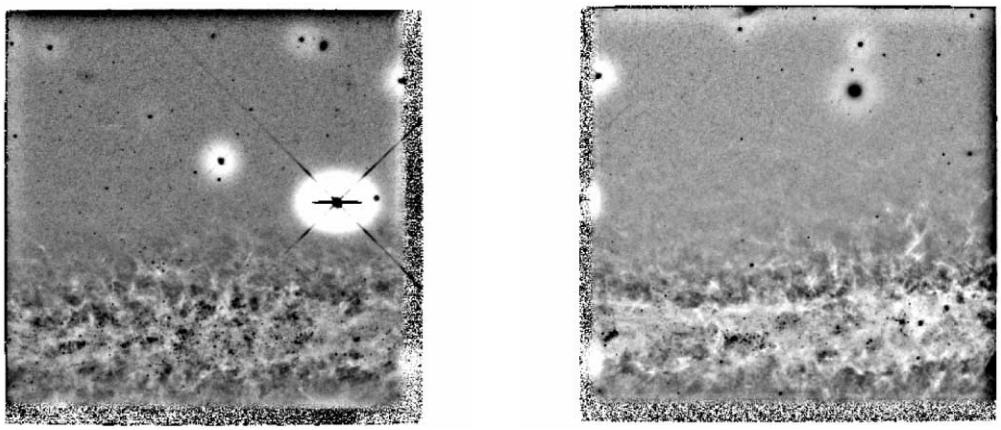

FIG. 9.—Unsharp-masked F675W image of the WF4 field (*left*) and WF3 field (*right*), revealing many individual dust filaments. The image is oriented with the galactic plane being parallel (rotated by 90° to previous figures) for convenience.

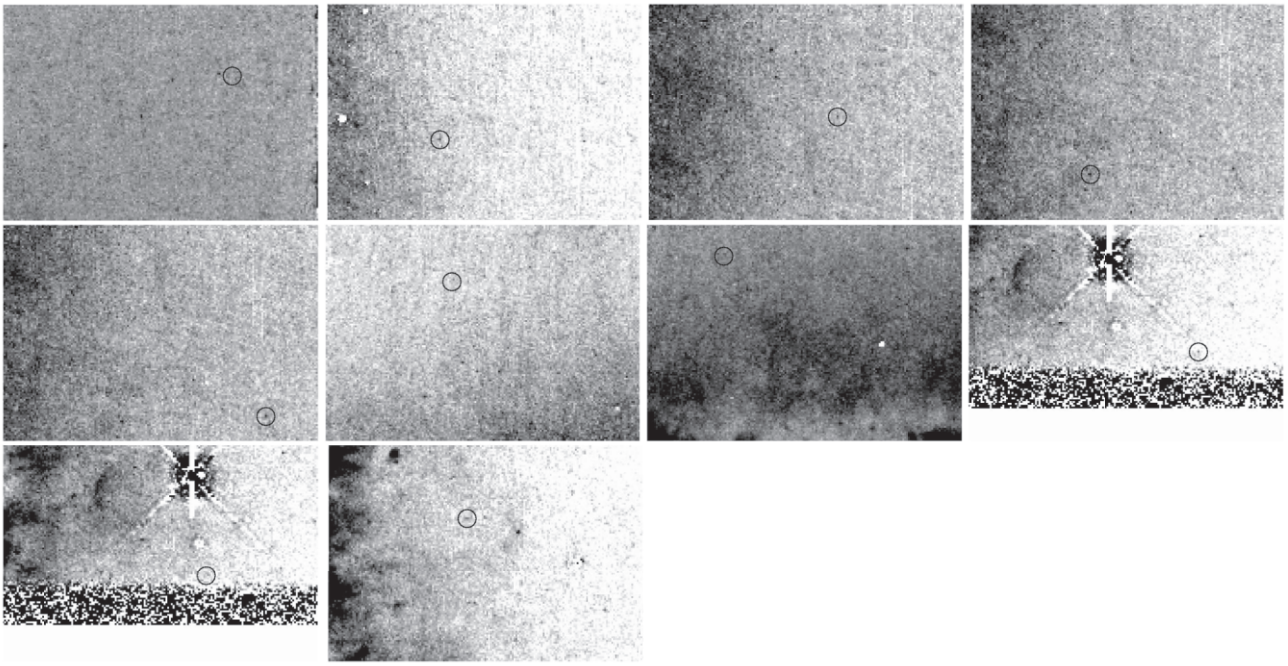

FIG. 10.—Ten candidate halo PNs in our four WF/PC fields. The positions of the PNs are marked by black circles. From top left to bottom middle, we show the fields of the PNs 33, 20, 26, 01, 04, 11, 03, 24, 25, and 13 of Ciardullo et al. (1991).

Although the detections by Ciardullo et al. (1991) were based on the [O III] emission line flux, which is usually the strongest emission line in PNs, those species often also exhibit a considerable amount of Hα emission. We list the properties of the PNs in Table 4, including identifier, position, size, and distance from the midplane. The identifier is a combination of the WF/PC field and the running order sorted by right ascension for each of the four WF/PC fields. Of the 10 candidate PNs, we marginally detected six, with only two clear detections. From one of those two (PN-WF2-4), we estimated the flux in an aperture with a radius of 0.″5 pixels, which yielded a magnitude of $m_{\rm F656N} = 26.13 \pm 0.01$, which corresponds roughly to the limiting magnitude of a point source we reached in our Hα observation.

7. COMPARISON WITH OTHER MULTIFREQUENCY HIGH SPATIAL RESOLUTION DATA

7.1. *Optical versus NIR Narrowband Imagery*

The detailed investigation of the connection between the superbubbles and the filaments that are driven by outflows can be achieved by NIR narrowband observations, which reveal star formation regions (eg., in the Brγ or Paα line). We have looked at the *HST* archival NICMOS Paα observation of NGC 891 for a detailed analysis of the disk-halo interface in NGC 891. These observations were part of the wide-field Paα snapshot survey of nearby galaxy nuclear regions (PI: W. Sparks) and have previously been published by Böker et al. (1999). The field of view of the NICMOS image is substantially (about a factor of 9) smaller (51.″2 × 51.″2) compared with our WFPC2 image of NGC 891. Unfortunately, the offsets of the image centers between the NICMOS and WFPC2 observations amount to $\Delta\alpha = +19.''5$ and $\Delta\delta = -81.''0$ and hence show only a very marginal overlap.

The Paα 1.875 μm line observations trace the regions deep within the disk that are almost obscured at optical wavelengths because of the prominent dust lane. The image shows only a few brighter star-forming regions within the disk and a moderately bright nuclear region. There is still a considerable amount of dust visible as well. As this pointing traces the nuclear part of NGC 891, where a substantial decrease in Hα emission was already visible from ground-based images, this confirms that there is much less star formation happening at, and surrounding, the nuclear regions compared with the brighter emission

TABLE 4

PLANETARY NEBULAE IN THE HALO OF NGC 891

Identifier	R.A. (J2000.0)	Decl. (J2000.0)	$\lvert z\rvert$ (pc)	Size	Detect.	Alternate Name
PN-PC-1	02 22 38.96	+42 22 25.5	1105	...	No	CJH91 No. 33
PN-WF2-1	02 22 29.67	+42 22 21.9	1161	Unresolved	Yes	CJH91 No. 20
PN-WF2-2	02 22 37.81	+42 21 26.7	1520	Unresolved	Yes	CJH91 No. 26
PN-WF2-3	02 22 37.90	+42 21 48.7	1161	Unresolved	Yes	CJH91 No. 01
PN-WF2-4	02 22 39.20	+42 21 42.5	1934	Unresolved	Yes	CJH91 No. 04
PN-WF3-1	02 22 31.80	+42 21 46.7	1879	...	No	CJH91 No. 11
PN-WF3-2	02 22 33.71	+42 22 03.3	1216	...	No	CJH91 No. 03
PN-WF4-1	02 22 33.08	+42 22 20.6	1838	Unresolved	Yes	CJH91 No. 24
PN-WF4-2	02 22 33.73	+42 22 17.1	1442	...	No	CJH91 No. 25
PN-WF4-3	02 22 35.56	+42 22 49.7	1133	Unresolved	Yes	CJH91 No. 13

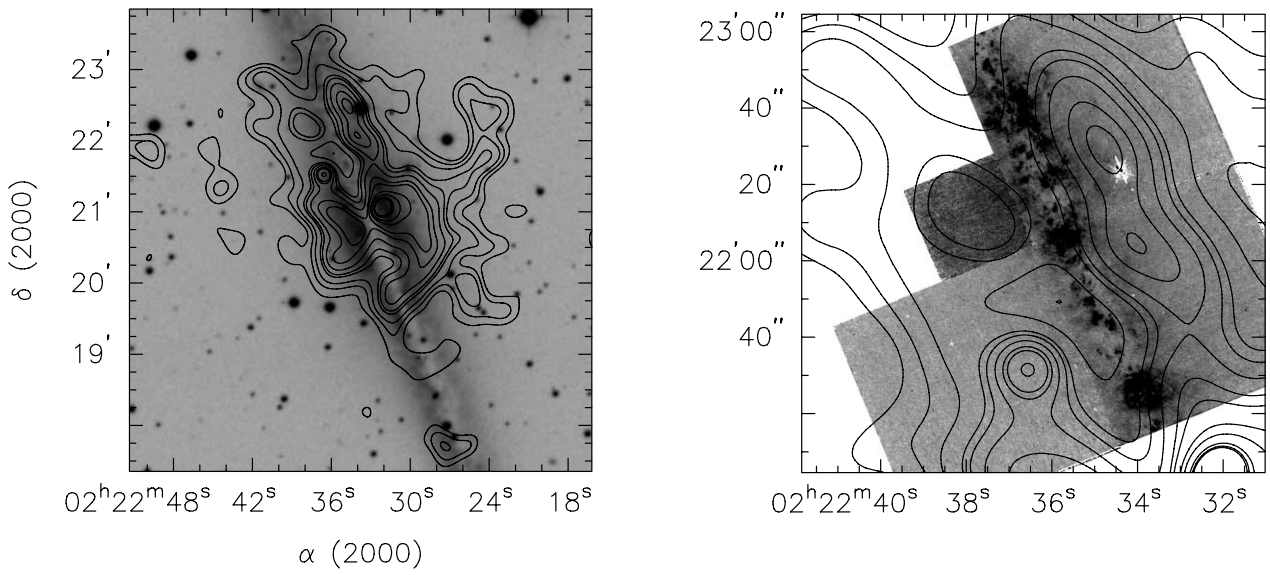

FIG. 11.—*Left*: DSS image of NGC 891 superposed with the *Chandra* ACIS soft X-ray contours in the 0.3–2.0 keV band. Contour levels are 1, 1.5, 2, 2.7, 3, 3.5, 4.1, 4.5, 5.5, 6.5, 8.5, 9.5, 10, 20, and 50 in units of 10^{-9} photons s^{-1} cm^{-2} $arcsec^{-2}$ ($pixel^{-1}$). *Right*: More detailed view with our WFPC2 Hα image.

regions in the northern part of NGC 891 (e.g., Dettmar 1990; Rand et al. 1990).

7.2. *A Detailed Comparison with Chandra X-Ray Data*

NGC 891 has been studied in the X-ray regime with *ROSAT* (Bregman & Pildis 1994), with which an extended X-ray halo has been detected. More recently, in a sample of star-forming disk galaxies the spatial and spectral properties of NGC 891 have been thoroughly investigated (Strickland et al. 2004a, 2004b). We used the *Chandra* ACIS image of Strickland et al. (2004a) to compare the small scale structure of the hot ionized medium with the warm ionized medium. In Figure 11 we show the superposition of the two ISM constituents. The left panel shows the DSS image of NGC 891 superposed with the contours of the *Chandra* ACIS observation. The *Chandra* image shows the soft X-ray emission in the 0.3–2.0 keV band, which has been background-subtracted and adaptively smoothed to achieve a better S/N. The point sources have been removed as well. For further details on the X-ray observations and reductions, see Strickland et al. (2004a). In the right-hand panel we show the superposition of our WFPC2 Hα image, again with the *Chandra* ACIS soft 0.3–2.0 keV band. The global distribution of the X-ray emission follows the north-south asymmetry, which was also observed in Hα (e.g., Dettmar 1990; Rossa & Dettmar 2003b) and in the radio continuum (e.g., Dahlem et al. 1994).

The disk of NGC 891 lacks strong X-ray emission, although it is embedded in a pervasive soft X-ray layer. However, two local maxima in the 0.3–2.0 keV band were detected in the northwestern halo region above strong supershells in the disk. This is also the halo region ($|z| \geq 1$ kpc), where our diffuse Hα emission is brightest. The pipeline-processed *XMM-Newton* EPIC pn-image shows more or less the same global structure as the *Chandra* image.

8. DISCUSSION

The general eDIG morphology of previous ground-based observations of the disk-halo interface in NGC 891 is recovered (e.g., Dettmar 1990; Rand et al. 1990). However, our high spatial resolution observation reveals an interesting substructure that has eluded ground-based observations. A pervasive eDIG layer is detected. The observed Hα morphology in NGC 891 is mostly diffuse, suggesting that a breakup of the homogeneous layer may only occur at very faint intensities with associated EMs of less than 20 cm^{-6} pc. Several faint filaments are detected, which reach very high galactic latitudes $|z| \sim 2$ kpc. Some of these filaments are very collimated and show no considerable broadening toward high-$|z|$. This may indicate that magnetic fields have a strong influence on those features and in turn can play a vital role as the transport mechanism. Since we do not see much evidence for the chimney scenario, other mechanisms have to be considered. As dust is also detected at high-$|z|$, though it is not spatially correlated with the eDIG on a one-to-one basis, soft mechanisms for the transport of the dust are favored, such as photolevitation (Franco et al. 1991; Ferrara et al. 1991) or, possibly, magnetic field instabilities (Parker 1992; Shchekinov et al. 2001). However, which of the processes act as the actual transport of the dust features is not yet known. Whereas the eDIG morphology is smoothly distributed, the dusty ISM phase shows much more substructure and is generally very clumpy. In fact, a very intricate network of dust features is observed, which shows an irregular pattern. The detected ionized structures (i.e., the supergiant shells) in the galactic midplane—in contrast to the high-$|z|$ dusty filaments—are comparable in size and shape to Milky Way analogues (e.g., Heiles 1984; Koo et al. 1992).

One of the key results of our study is that the DIG does not break up into many chimneys at the heights above the disk where we can see it. More specifically, this is true for our spatial resolution and sensitivity limits (5 pc width and a surface brightness above 20 cm^{-6} pc). This can be for various reasons. It is possible that the medium is intrinsically too unorganized (i.e., inhomogeneous) for organized structures like chimneys to survive or to be formed in the first place. That is, the outflow of hot gas occurs mostly through an irregular medium, maybe fractal in nature (e.g., Elmegreen 1998), such that the energy can get out so quickly that the expected formation of walls is not happening at all. It has been argued that

only in starbursts is sufficient energy produced locally for matter to be piled up in chimneys (Wills et al. 1999).

The lack of correlation of dust and Hα filaments may also point to a much more chaotic medium than could be modeled in the chimney scenario. On the other hand, the dust appears more filamentary than the Hα. This could be due to the difference in morphology. We are likely seeing preferentially denser dust features and not the diffuse dust.

Given the sensitivity limit of EM = 20 cm^{-6} pc, we can roughly estimate the kind of chimney wall, seen edge-on, that this would correspond to. Our spatial resolution limit is 5 pc. An assumed 20 pc long chimney wall requires a medium with a density of $n_e = 1$ cm^{-3}. This is not regarded as a very dense medium. If the density is to be much higher, the chimney wall would have to be much thinner or the path length along it much shorter than 20 pc. Alternatively, the chimneys might indeed be there, *but only* closer to the disk where we cannot see them, possibly because of heavy dust obscuration.

The outflow, as in a starburst galaxy, is dominated by a few major complexes, which we indeed also see below the few longer filaments in NGC 891. These could be chimney walls or remnants of chimney walls. Alternatively, the larger filaments could indicate some large-scale magnetic field topology, in which the magnetic field, not necessarily the chimneys, would be responsible for the organization of matter in them. To vindicate or refute this conjecture, much higher spatial resolution and higher sensitivity radio continuum observations are mandatory.

8.1. *Collimated Filaments: Magnetically Confined?*

Quite surprisingly, we discerned a few very narrow filaments, which are well collimated even at high galactic latitudes. The chimney structures, or at least the walls of chimneys, which would be observationally visible as dust pillars, should show a widening with increasing distance from the galactic midplane. However, we do not see such structures in our Hα image. Instead, these very collimated long filaments seem to originate from the bright superbubbles in the galactic midplane. In a Milky Way study Haffner et al. (1998) found two very collimated long filaments based on sensitive observations carried out with the WHAM. One of the two faint filaments they discovered is 80° long (corresponding to a length of about 1.2 kpc above the midplane). It has a nearly constant Hα intensity profile of EM $\approx$ 1.1 cm^{-6} pc. Although the origin of the filaments is not quite clear, it has been speculated that a jetlike ejection from the CMa R1/OB1 association is responsible, but other mechanisms seem possible too (Haffner et al. 1998). So it may well be that the filaments seen in the Milky Way and those we identified in NGC 891 have a similar, yet unknown origin.

In a study of NGC 891 by Scarrott & Draper (1996) they used optical polarization measurements, and they found vertical magnetic fields in the halo region above the inner part (i.e., the bulge region). This finding prompted speculation about an optical spur like the north Galactic spur known in the Milky Way (Mathewson & Ford 1970). However, optical polarization measurements face challenges, as it might be difficult, if not impossible, to disentangle whether the polarization is due to grain alignment or to dust scattering. Quite interestingly, the maximum polarization vector (perpendicular to the disk) in these observations (Scarrott & Draper 1996) is close to the position above our detected supergiant shell, from which the collimated features rise into the halo.

9. SUMMARY

We have presented new high spatial resolution narrowband observations of eDIG in the nearby edge-on galaxy NGC 891, obtained with the WFPC2 on board *HST*. A region 6.9 kpc $\times$ 6.9 kpc in size centered on the northeastern part of NGC 891 was investigated. An extraplanar layer with an extension of at least 1.8 kpc above/below the galactic midplane was found. Superposed onto this eDIG layer are several filaments and arcs, reaching extraplanar distances of about $|z| \approx 2.2$ kpc. A few superthin, and collimated filaments were detected, which have a surprisingly high length/width ratio of up to $l/b \sim 140$! Most of the Hα emission is diffuse, although several discrete emission features are detected. Whereas the observed global morphology validates the results of previous ground-based observations, the high spatial resolution observations reveal local structures that have not been resolved or detected by ground-based optical observations. The mechanisms of the gas and energy transport into the halo cannot be verified without ambiguity; however, the chimney scenario is most likely not responsible for the transport, as no clear structures representing individual chimneys (i.e., the walls of chimneys) have been detected. The highly collimated gaseous filaments suggest the influence of magnetic fields. We have further presented results of yet another constituent of the ISM, the dust in the disk-halo interface of NGC 891.

Extraplanar dust was detected and has been analyzed from the unsharp-masked broadband image. The observations reveal extraplanar dust at high galactic latitudes, as previously reported by (Howk & Savage 1997, 2000). We detected dusty filaments up to $|z| \sim 2$ kpc above the galactic midplane. Although there is a correlation observed between the *two* different ISM constituents, as both constituents are detected in the halo of NGC 891, generally no one-to-one correlation between individual filaments and dust filaments is observed. The dust morphology is twofold. Many dust filaments are aligned perpendicular to the galactic disk, indicating that magnetic fields may play a key role in transporting the dust into the disk-halo interface. Other dusty filaments, however, located mostly at the highest galactic latitudes, are aligned parallel to the disk, which may represent a temporal equilibrium of the dusty ISM phase, possibly transported by soft mechanisms (e.g., photolevitation) into the galactic halo.

The spatial distribution of the soft X-ray emission in the halo of NGC 891, as revealed by *Chandra*, is in good agreement with our Hα observations. There are two local maxima of X-ray emission in the halo, where also the diffuse Hα emission is strongest.

We would like to thank David Strickland for providing us with the calibrated *Chandra* ACIS image of NGC 891. We also thank the anonymous referee for a swift report and helpful comments, which improved the clarity of the paper in a few places. The authors (J. R. and R. J. D.) acknowledge financial support for this research project by the Deutsches Zentrum für Luft- und Raumfahrt through grant 50 OR 9707.

REFERENCES

Alton, P. B., Bianchi, S., Rand, R. J., Xilouris, E. M., Davies, J. I., & Trewhella, M. 1998, ApJ, 507, L125
Birk, G. T., Lesch, H., & Neukirch, T. 1998, MNRAS, 296, 165
Böker, T., et al. 1999, ApJS, 124, 95
Bregman, J. H., & Pildis, R. A. 1994, ApJ, 420, 570
Cecil, G., Bland-Hawthorn, J., & Veilleux, S. 2002, ApJ, 576, 745
Cecil, G., Bland-Hawthorn, J., Veilleux, S., & Filippenko, A. V. 2001, ApJ, 555, 338
Ciardullo, R., Jacoby, G. H., & Harris, W. H. 1991, ApJ, 383, 487
Chevalier, R. A., & Clegg, A. W. 1985, Nature, 317, 44
Collins, J. A., Rand, R. J., Duric, N., & Walterbos, R. A. M. 2000, ApJ, 536, 645
Dahlem, M., Dettmar, R.-J., & Hummel, E. 1994, A&A, 290, 384
de Avillez, M. A. 2000, MNRAS, 315, 479
Dettmar, R.-J. 1990, A&A, 232, L15
Dettmar, R.-J., & Schulz, H. 1992, A&A, 254, L25
Domgörgen, H., & Mathis, J. S. 1994, ApJ, 428, 647
Dove, J. B., & Shull, J. M. 1994, ApJ, 430, 222
Elmegreen, B. G. 1998, Publ. Astron. Soc. Australia, 15, 74
Ferguson, A. M. N., Wyse, R. F. G., & Gallagher, J. S. 1996a, AJ, 112, 2567
Ferguson, A. M. N., Wyse, R. F. G., Gallagher, J. S., & Hunter, D. A. 1996b, AJ, 111, 2265
Ferrara, A., Bianchi, S., Dettmar, R.-J., & Giovanardi, C. 1996, ApJ, 467, L69
Ferrara, A., Ferrini, F., Barsella, B., & Franco, J. 1991, ApJ, 381, 137
Franco, J., Ferrini, F., Barsella, B., & Ferrara, A. 1991, ApJ, 366, 443
Fruchter, A. S., & Hook, R. N. 2002, PASP, 114, 144
García-Burillo, S., Guélin, M., Cernicharo, J., & Dahlem, M. 1992, A&A, 266, 21
Gaustad, J. E., McCullough, P. R., Rosing, W., & Van Buren, D. 2001, PASP, 113, 1326
Gerhard, O., Arnaboldi, M., Freeman, K. C., & Okamura, S. 2002, ApJ, 580, L121
Gonzaga, S., et al. (STScI WFPC2 Group). 1998, The Drizzling Cookbook (Instr. Sci. Rep. WFPC2 98-04) (Baltimore: STScI)
Haffner, L. M., Reynolds, R. J., & Tufte, S. L. 1998, ApJ, 501, L83
Haffner, L. M., Reynolds, R. J., Tufte, S. L., Madsen, G. J., Jaehnig, K. P., & Percival, J. W. 2003, ApJS, 149, 405
Hambly, N. C., et al. 1996, A&A, 306, 119
Heiles, C. 1984, ApJS, 55, 585
Hoopes, C. G., Walterbos, R. A. M., & Rand, R. J. 1999, ApJ, 522, 669
Howk, J. C., & Savage, B. D. 1997, AJ, 114, 2463
———. 1999, AJ, 117, 2077
———. 2000, AJ, 119, 644
Kennicutt, R. C., Jr. 1988, ApJ, 334, 144
Keppel, J. W., Dettmar, R.-J., Gallagher, J. S., III, & Roberts, M. S. 1991, ApJ, 374, 507
Kilkenny, D., Luvhimbi, E., O'Donoghue, D., Stobie, R. S., Koen, C., & Chen, A. 1995, MNRAS, 276, 906
Koo, B.-C., Heiles, C., & Reach, W. T. 1992, ApJ, 390, 108
Korpi, M. J., Brandenburg, A., Shukurov, A., Tuominen, I., & Nordlund, Å. 1999, ApJ, 514, L99
Lehnert, M. D., & Heckman, T. M. 1995, ApJS, 97, 89
Mathewson, D. S., & Ford, V. L. 1970, MmRAS, 74, 139
Mathis, J. S. 1986, ApJ, 301, 423
Meaburn, J. 1980, MNRAS, 192, 365
Miller, S. T., & Veilleux, S. 2003, ApJS, 148, 383
Miller, W. W., III, & Cox, D. P. 1993, ApJ, 417, 579
Norman, C. A., & Ikeuchi, S. 1989, ApJ, 345, 372
O'Dell, C. R., & Doi, T. 1999, PASP, 111, 1316
Parker, E. N. 1992, ApJ, 401, 137
Pildis, R. A., Bregman, J. N., & Schombert, J. M. 1994, ApJ, 427, 160
Popescu, C. C., Tuffs, R. J., Kylafis, N. D., & Madore, B. F. 2004, A&A, 414, 45
Rand, R. J. 1996, ApJ, 462, 712
———. 1997, ApJ, 474, 129
———. 1998, ApJ, 501, 137
———. 2000, ApJ, 537, L13
Rand, R. J., Kulkarni, S. R., & Hester, J. J. 1990, ApJ, 352, L1
Reynolds, R. J. 1984, ApJ, 282, 191
Reynolds, R. J., Sterling, N. C., Haffner, L. M., & Tufte, S. L. 2001, ApJ, 548, L221
Rossa, J., & Dettmar, R.-J. 2000, A&A, 359, 433
———. 2003a, A&A, 406, 493
———. 2003b, A&A, 406, 505
Rupen, M. P. 1991, AJ, 102, 48
Ryan-Weber, E. V., et al. (SINGG Team). 2004, AJ, 127, 1431
Scarrott, S. M., & Draper, P. W. 1996, MNRAS, 278, 519
Shapiro, P. R., & Field, G. B. 1976, ApJ, 205, 762
Shchekinov, Y. A., Dettmar, R.-J., Schröer, A., & Steinacker, A. 2001, Astron. Astrophys. Trans., 20, 237
Slavin, J. D., Shull, J. M., & Begelman, M. C. 1993, ApJ, 407, 83
Strickland, D. K., Heckman, T. M., Colbert, E. J. M., Hoopes, C. G., & Weaver, K. A. 2004a, ApJS, 151, 193
———. 2004b, ApJ, 606, 829
Swaters, R. A., Sancisi, R., & van der Hulst, J. M. 1997, ApJ, 491, 140
Thilker, D. A., Walterbos, R. A. M., Braun, R., & Hoopes, C. G. 2002, AJ, 124, 3118
Tüllmann, R., Dettmar, R.-J., Soida, M., Urbanik, M., & Rossa, J. 2000, A&A, 364, L36
Tüllmann, R., Rosa, M. R., Elwert, T., Bomans, D. J., Ferguson, A. M. N., & Dettmar, R.-J. 2003, A&A, 412, 69
van den Bergh, S. 1992, PASP, 104, 861
Wada, K. 2001, ApJ, 559, L41
Wada, K., & Norman, C. A. 1999, ApJ, 516, L13
———. 2001, ApJ, 547, 172
Walterbos, R. A. M., & Braun, R. 1994, ApJ, 431, 156
Wang, Q. D., Immler, S., Walterbos, R. A. M., Lauroesch, J. T., & Breitschwerdt, D. 2001, ApJ, 555, L99
Wills, K. A., Redman, M. P., Muxlow, T. W. B., & Pedlar, A. 1999, MNRAS, 309, 395